GPS determination of the velocity and strain-rate fields on Schirmacher Glacier, central Dronning Maud Land, Antarctica

P.S. SUNIL,[1] C.D. REDDY,[1] M. PONRAJ,[1] Ajay DHAR,[1] D. JAYAPAUL[2]

[1]*Indian Institute of Geomagnetism, New Panvel, New Bombay 410218, India*
E-mail: sunilps@iigs.iigm.res.in
[2]*Antarctic Division, Geological Survey of India, Faridabad 121001, India*

ABSTRACT. Global positioning system (GPS) campaigns were conducted during the 2003 and 2004 austral summer seasons to obtain insight into the velocity and strain-rate distribution on Schirmacher Glacier, central Dronning Maud Land, East Antarctica. GPS data were collected at 21 sites and analyzed to estimate the site coordinates, baselines and velocities. The short-term precision of the base station, MAIT, is estimated from the daily coordinate repeatability solutions during the two years. All GPS points on the glacier were constrained with respect to MAIT and nearby International GPS Service stations. Horizontal velocities of the glacier sites lie between 1.89 ± 0.01 and $10.88 \pm 0.01 \, \mathrm{m \, a^{-1}}$ to the north-northeast, with an average velocity of $6.21 \pm 0.01 \, \mathrm{m \, a^{-1}}$. The principal strain rates provide a quantitative measurement of extension rates, which range from $(0.11 \pm 0.01) \times 10^{-3}$ to $(1.48 \pm 0.85) \times 10^{-3} \, \mathrm{a^{-1}}$, and shortening rates, which range from $(0.04 \pm 0.02) \times 10^{-3}$ to $(0.96 \pm 0.16) \times 10^{-3} \, \mathrm{a^{-1}}$. The velocity and strain-rate distributions across the GPS network in Schirmacher Glacier are spatially correlated with topography, subsurface undulations, fracture zones/crevasses and the partial blockage of the flow by nunataks and the Schirmacher Oasis.

INTRODUCTION

The polar regions are important components of the global environment. Antarctic ice, which contains 90% of the world's total ice (70% of the freshwater ice), plays an active role in global climatic change, and estimating the glacier dynamics is essential for understanding the mass balance of the Antarctic ice sheet (Gloersen and Campbell, 1988; Meir, 1993; Wingham and others, 1998). Some 90% of the discharge from the Antarctic ice sheet is through a small number of ice streams and outlet glaciers. Understanding the complex dynamics of these drainage systems requires fundamental information, such as surface mass balance, depth and temperature of the ice, meteorological conditions, surface velocity vectors, strain rates, surface gradients and changes in surface elevation. Some of these important outlet glaciers have been studied (e.g. ice velocity observations on Potsdam Glacier (Dietrich and others, 1999; Metzig and others, 2000; Anschütz and others, 2007), Lambert Glacier (Manson and others, 2000; Testut and others, 2003), the Amery Ice Shelf (King, 2001; Bassis and others, 2005; Fricker and others, 2005), Shirase Glacier (Pattyn and Naruse, 2003), Pine Island Glacier (Joughin and others, 2003) and the Larsen B ice shelf (Rignot and others, 2004). Schirmacher Glacier makes a major contribution to the drainage of coastal East Antarctica, being an important outlet glacier in central Dronning Maud Land.

Prior to the mid-1970s, ice flow velocities were measured using astronomical positioning techniques (e.g. Liebert and Leonhardt, 1973) and stake readings. With advances in airborne and space-borne geodetic techniques, it is now feasible to monitor glacier velocities and strain rates very precisely (King, 2004). There are several well-established space-borne geodetic techniques for this purpose, including global positioning system (GPS) (Leick, 1995), interferometric synthetic aperture radar (InSAR) (Goldstein and others, 1993) and the Ice, Cloud and land Elevation satellite

(ICESat) (Zwally and others, 2002). Amongst these, GPS remains an indispensable tool for a comprehensive understanding of ice kinematics. Korth and Dietrich (1996), Dietrich and others (1999), Metzig and others (2000) and M. Scheinert (unpublished information) outline a variety of geodetic observation techniques, which have been applied in investigations of geodynamic phenomena in the Schirmacher Oasis region. Here, we describe the velocity and strain-rate fields obtained during two GPS campaigns undertaken on Schirmacher Glacier during the summer seasons of 2003 and 2004.

GEODYNAMIC SETTINGS

Schirmacher Glacier in central Dronning Maud Land (Fig. 1) is part of the Antarctic rift system that has evolved in different stages since the Gondwanaland break-up in Jurassic time (Lawver and others, 1992). It is located between an area south of the Lazarev Sea and Nivlisen ice shelf (Sengupta, 1986; Hermichen, 1995; Horwath and others, 2006) and north of Potsdam Glacier and the Wohlthat Mountains; Anschütz and others 2007). The study region is bounded by latitudes 70°40′ S and 71°00′ S and longitudes 11°10′ E and 12°10′ E. Mean annual air temperature is below –20°C (Bormann and Fritzsche, 1995). In general terms, the Schirmacher Glacier flow is blocked by the Schirmacher Oasis (a low-lying nunatak) located to the north.

The study area is divided into three distinct topographic units: the southern continental ice sheet, elevated nunataks and, to the north, shelf ice which exhibits distinct surface undulations (Ravindra and others, 2002). The region is also characterized by gentle to steep gradient surface slopes with some subglacial highs and lows above mean sea level (Damm and Eisenburger, 2005; Meyer and others, 2005), criss-cross fractures and crevasses close to the Schirmacher Oasis. To the north of Schirmacher Oasis there is shelf ice
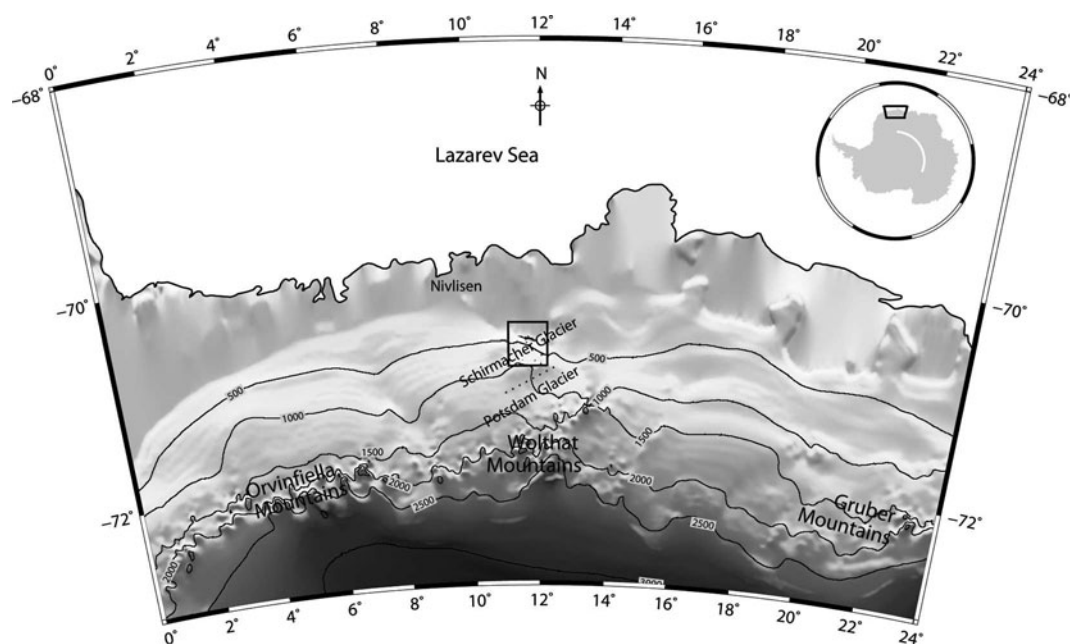
Fig. 1. Location map of central Dronning Maud Land, East Antarctica, showing the study area of Schirmacher Glacier (rectangle) superimposed on a shaded relief map of GTOPO30 digital elevation model with 500 m elevation contour interval. Dotted line below the rectangle indicates the location of ground-penetrating radar (GPR) profiles by Anschütz and others (2007).

exhibiting pressure ridges. A large ablation area is located in the south-southeast, which extends to the Wohlthat Mountains (Bormann and Fritzsche, 1995).

SURVEY DESCRIPTION AND DATA PROCESSING

The GPS network on Schirmacher Glacier consists of 21 sites with ~5 km inter-station spacing (Fig. 4). At all sites in the network, GPS data were collected using dual-frequency (L1/L2) geodetic Trimble 4000SSi receivers with choke ring antennae, during January to March in 2003 and 2004. In the second campaign, only 15 sites (out of 21) were re-occupied, as some were lost/untraced due to accumulation of fresh snow. Each antenna was fixed on a 1.5 cm diameter threaded steel bolt fixed on a wooden block of 0.5 m × 0.5 m, embedded to a depth of 0.75 m in the ice (Fig. 2a). All the sites were observed continuously for 48–72 hours with 30 s sampling interval and 15° elevation mask. The base station (MAIT) was set up on exposed bedrock near the Indian Antarctic Research Station, Maitri, which is ~15 km away from the survey region (Figs 2b and 4). The GPS receivers in the field were powered by specially sealed 12 V, 72 Ah charged batteries enclosed in non-conducting boxes.

The recorded GPS data, organized into 24 hour segments, covered a Universal Time Coordinated (UTC) day and were analyzed in three steps. In the first step, the GPS carrier phase data were processed with the precise ephemeris from the International GPS Service (IGS) stations to produce position estimates and an associated covariance matrix of loosely constrained daily solutions for station positions using GPS Analysis Massachusetts Institute of Technology (GAMIT) software (King and Bock, 2002). In the next step these loose-ly constrained regional solutions were combined with global solutions produced by the Scripps Orbit and Permanent Array Center, San Diego, California, USA, using the Global Kalman filter (GLOBK) program (Herring, 2002). The basic algorithms and a description of this technique are given by Herring and King (1990), and its application to GPS data is given by Feigl and others (1993). Station position and velocity vectors at each site were obtained from these combined quasi-observations (Dong and others, 1998) in the third step. Since the velocity of the glaciers is very high compared to crustal movement, we consider only the MAIT base station and nearby global IGS stations, SYOG and VESL to constrain the glacier velocity solutions in International Terrestrial Reference Frame (ITRF2000) (Altamimi and others, 2002).
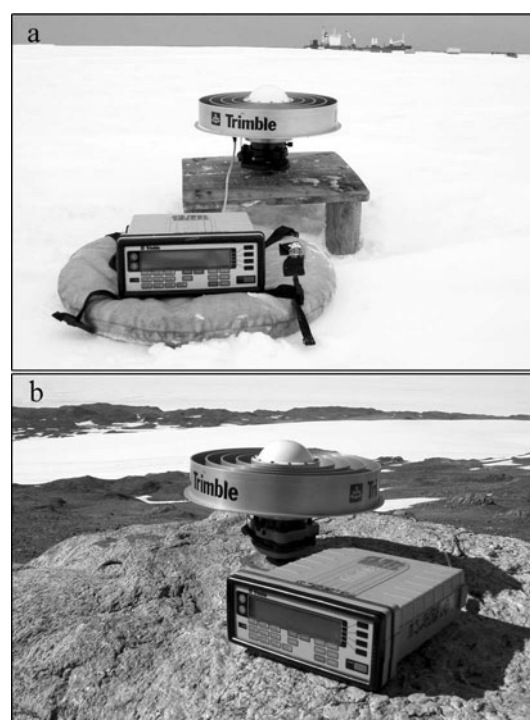
Fig. 2. (a) GPS antenna mounted on wooden platform on the glacier. (b) Set-up of the GPS base station on bedrock.
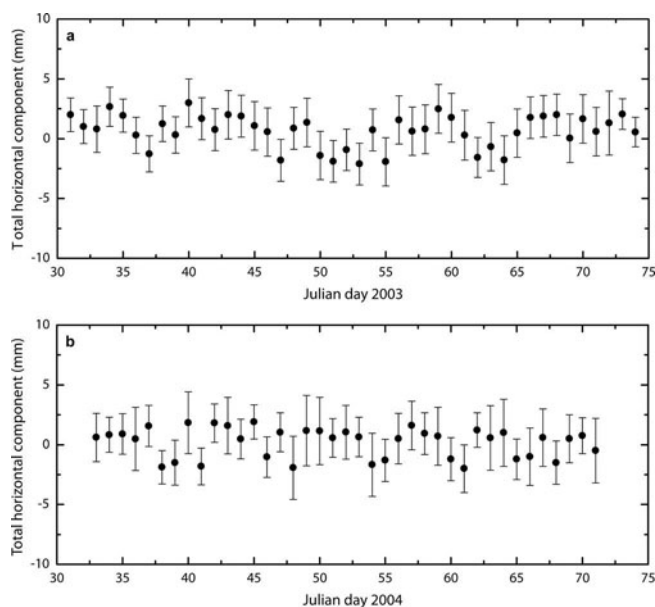
Fig. 3. Total horizontal component time series of base station (shown in Fig. 2b), for campaigns during (a) 2003 and (b) 2004.

BASE STATION REPEATABILITY

In GPS studies, the consistency/stability of the base station is very important, particularly in the Antarctic, where glacial load and ice flow can cause crustal deformation. The precision of the sites is assured provided the base station has high repeatability in the position coordinates. To improve the ambiguity resolution of the MAIT base station, data from the nearby IGS stations (OHI2, SYOG, VESL and MAW1) were imposed by putting tight constraints (3–5 mm in the horizontal, 5–10 mm in the vertical) on their a priori coordinate values in the ITRF2000 frame. At MAIT the coordinates were

allowed to vary freely by way of very loose constraints (10 m) to avoid singularity in the normal matrix (Dong and others, 1998). The short-term precision of the MAIT position is estimated from the daily solution repeatability (with corresponding rms) separately for the two campaigns.

To check the repeatability of the MAIT position, 44 days of data during 2003 (Julian days 31–74) and 39 days of data during 2004 (Julian days 33–71) have been used. The daily coordinates were obtained by considering wet tropospheric zenith delay (Vey and others, 2002), ionospheric free-linear combination (Davies and Hartmann, 1997), real valued carrier phase ambiguities, latitude-dependent variation (King and others, 2003) and satellite and receiver clock errors. Due to the satellite constellation, the GPS-estimated vertical coordinates are less precise than the horizontal coordinates; here we focus only on the precise estimation of the horizontal component of the base station. Thus we estimate the horizontal repeatability of MAIT with rms limits of 1.80 and 2.03 mm for the first and second campaigns, respectively. Figure 3 shows the time-series plots of daily position variations (total horizontal component) for the base station during the two campaigns. As seen from Figure 3, the daily coordinates show neither a significant offset nor a change of trend. This indicates good stability and justifies the use of MAIT as the base station. For estimating ice velocities and positions, measurements were equally constrained with respect to MAIT and to the IGS stations by applying equal weights.

VELOCITY AND GLACIER FLOW

For a complete description of the flow field of a glacier, both the horizontal and vertical components of the velocity are required. However, as mentioned above, we confine our analysis to the horizontal velocity components. By imposing tight constraints (1 cm a^{-1}) on the horizontal

Table 1. Geodetic coordinates of the GPS stations on Schirmacher Glacier with horizontal flow rates (in ITRF2000 at epoch 2004.0), azimuth and uncertainty. The dashed lines indicate absence of flow rates due to the inability to reoccupy stations during the second campaign

GPS site	Longitude (east)	Latitude (south)	No. of occupations	Horizontal velocity m a^{-1}	Azimuth °	Uncertainty mm a^{-1}
01	11.441	−70.747	1	–	–	–
02	11.463	−70.755	2	02.37	34.30	5.65
03	11.488	−70.768	1	–	–	–
04	11.527	−70.781	2	04.33	34.14	6.63
05	11.571	−70.798	2	06.56	19.22	7.54
06	11.624	−70.797	2	06.97	19.05	7.77
07	11.671	−70.796	2	07.82	25.81	7.92
08	11.719	−70.800	1	–	–	–
09	11.763	−70.806	2	08.81	34.28	8.26
10	11.808	−70.818	1	–	–	–
11	11.789	−70.826	2	10.79	38.13	6.55
12	11.488	−70.867	2	04.85	28.08	6.41
13	11.453	−70.858	2	04.47	27.27	6.46
14	11.463	−70.855	1	–	–	–
15	11.511	−70.888	1	–	–	–
16	11.478	−70.926	2	02.84	26.78	8.38
17	11.637	−70.863	2	07.18	16.82	7.37
18	11.700	−70.885	2	10.88	30.56	9.48
19	11.746	−70.886	2	08.70	44.64	7.49
20	11.812	−70.946	2	04.69	41.07	8.40
21	11.859	−70.958	2	01.89	35.91	7.03
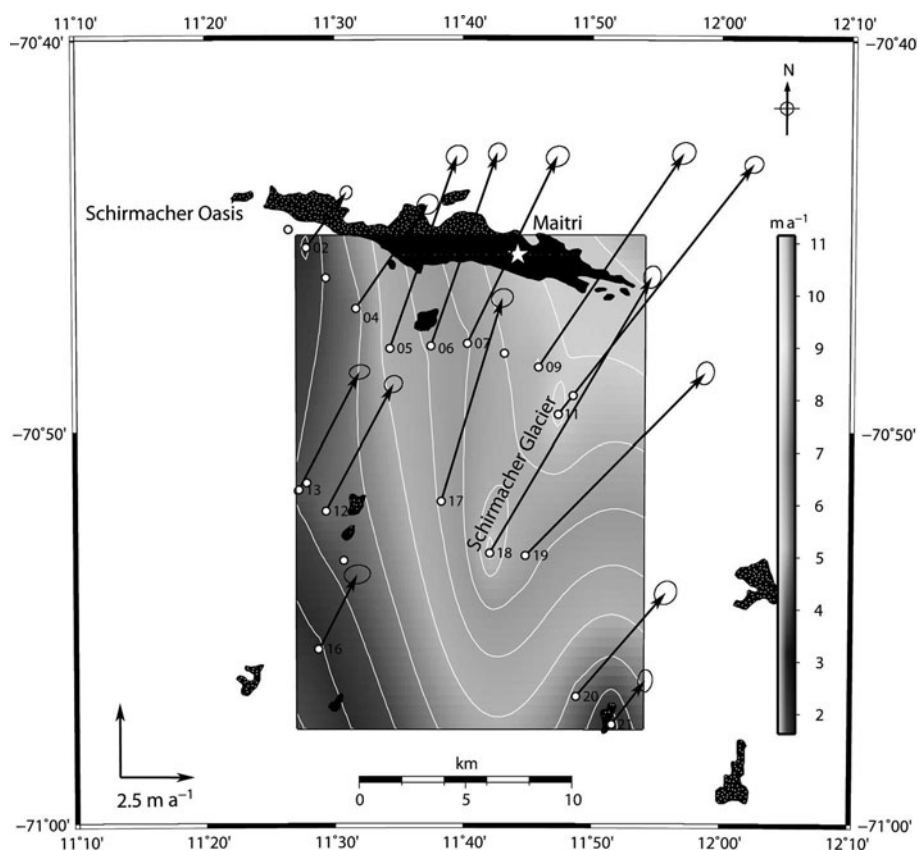
Fig. 4. Horizontal velocity vectors (with 95% confidence ellipses) for the GPS network on Schirmacher Glacier, superimposed on a shaded relief velocity-distribution map with 1 m contour interval obtained from the GPS velocity field. The scale represents the glacier flow rate corresponding to the velocity shaded relief (m a^{-1}). The black patches indicate the Schirmacher Oasis and nunataks.

components of the base station and the IGS sites, and relaxed constraints on glacier points (100 m a^{-1}), we obtained solutions for the horizontal velocity of Schirmacher Glacier. Table 1 gives the magnitude of the horizontal velocities (in ITRF2000 at epoch 2004.0) at various sites on Schirmacher Glacier.

The velocity vectors shown in Figure 4 represent the spatial pattern of glacier movement across Schirmacher Glacier. The lowest velocity, 1.89 ± 0.01 m a^{-1}, and highest, 10.88 ± 0.01 m a^{-1}, were observed in the southeastern and northeastern parts of the study area, respectively, with an average velocity of 6.21 ± 0.01 m a^{-1} in the north-northeast direction, with error limits of 95% confidence. The resulting velocities show that the eastern part of the Schirmacher Oasis acts to funnel Schirmacher Glacier toward Nivlisen. The GPS sites 02, 04, 05, 06 and 07 (Fig. 4), which are located over the continental slope with maximum steepness, exhibit low velocities, i.e. the velocity distribution is such that it is lowest near the Schirmacher Oasis margin and highest near the eastern part where the blockage of Schirmacher Oasis is absent. Overall, the velocity distribution shows that velocities decrease away from Schirmacher Oasis and towards the continental ice.

STRAIN-RATE ANALYSIS

While station velocities display absolute motion with respect to the reference frame and provide information on the kinematics of the glacier surface, strain rates provide information on the physics of how the ice flows, i.e. on the

deformational characteristics of the ice. Since triangulation techniques provide large spatial variability of the strain-rate pattern and are more sensitive to single station velocities and inter-site distances (Serpelloni and others, 2005) we divided the Schirmacher Glacier network into 18 triangular sub-networks to study the strain-rate distribution. Using a standard least-squares procedure (Feigl and others, 1990) we computed the horizontal strain-rate tensor within each region. Further, we derived the rates of shortening and elongation in the direction of the principal strain axes. The triangular regions and computed horizontal principal strain-rate axes are shown in Figure 5.

We computed the spatial distribution of the principal strain rate (ε) and the principal axis azimuth (ϕ) for the Schirmacher Glacier sites over a period of 1 year. The compressional strain rate (ε_{com}) ranges from $(0.04 \pm 0.01) \times 10^{-3}$ (triangle G) to $(0.96 \pm 0.16) \times 10^{-3}$ a^{-1}, with high compressional strain rates of $(0.84 \pm 0.23) \times 10^{-3}$, $(0.72 \pm 0.43) \times 10^{-3}$ and $(0.96 \pm 0.16) \times 10^{-3}$ a^{-1} observed in triangular regions A, C and M respectively. The extensional strain rates (ε_{ext}) are in the range $(0.02 \pm 0.01) \times 10^{-3}$ a^{-1} (triangle F) to $(1.48 \pm 0.85) \times 10^{-3}$ a^{-1} (triangle J). The east-west to north-northeast trending maximum extensional strains occur in the triangular regions H, J, K, Q and R, which are located in the eastern part of the glacier, where velocities are high. Very small compressional and extensional strain rates are found in triangle F. This pattern is due to acceleration along divergent flowlines in the east of Schirmacher Glacier. The calculated principal strain rates with azimuth and 1σ uncertainties are listed in Table 2.
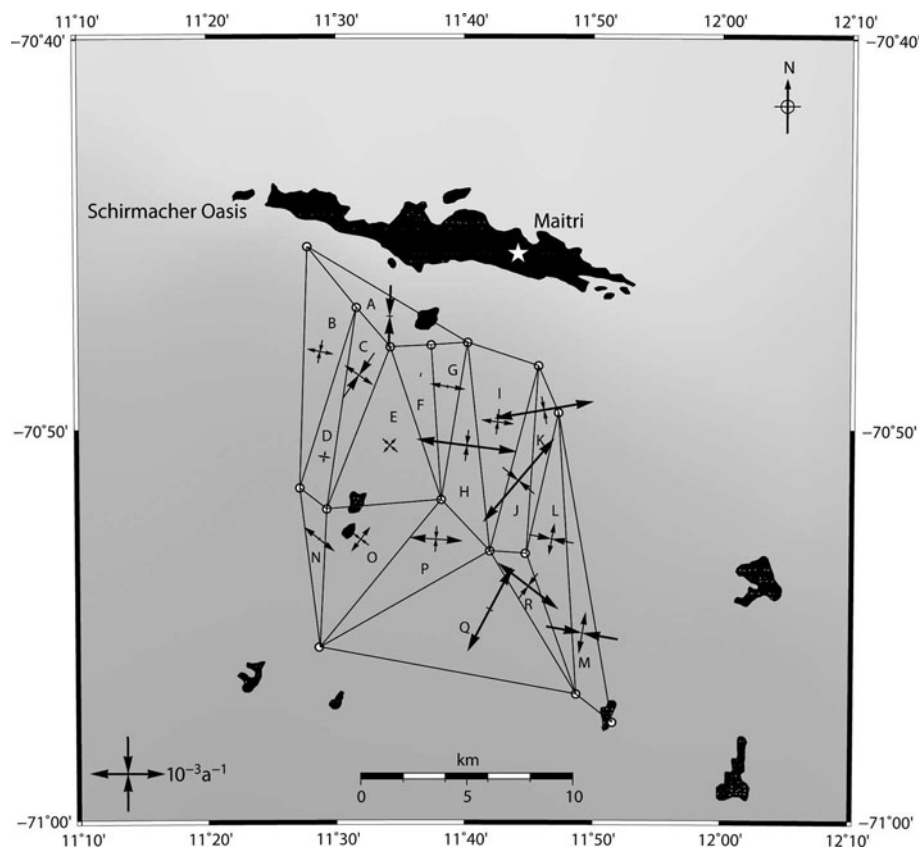
Fig. 5. Spatial distribution of the principal strain rates for triangular regions. The outward and inward arrows display extension and contraction, respectively. Coordinates of the barycentres of these triangles are given in Table 2.

DISCUSSION

The velocity distribution map (Fig. 4) with velocity magnitude contour, prepared from the measured station velocities, shows the trend of the glacier flow towards the north-northeast into Nivlisen. The map shows lesser velocities in the southwestern part of the area and a gradual increase up to a maximum of $\sim$11 m a^{-1} in the ice-shelf area towards the northeastern part of the glacier. The high-velocity region shown on the map consists of GPS sites 09, 11, 18 and 19. A gentle slope was observed in this region during the field survey and from the 30 arcsec global topographic (GTOPO30) digital elevation model; the maximum velocities seen in this part are due to the minimum blockage of the Schirmacher Oasis. At GPS sites 02, 04, 05, 06 and 07, despite their location over the steep elevation gradient region, the velocity is low; this is because of the resistance to flow due to the Schirmacher Oasis blockage. The results from this study agree with previous geodetic investigations (Dietrich and others, 1999; Metzig and others, 2000; M. Scheinert, unpublished information) carried out near this area and show that the major outlet of Schirmacher Glacier towards Nivlisen is through the eastern end of the Schirmacher Oasis. However, the general trend of the velocity pattern shows that, away from the Schirmacher Oasis towards the continental ice, the velocity decreases due to the very gentle slope in the continental ice surface and the presence of nunataks. A ground-penetrating radar (GPR) study conducted south of our study area, on Potsdam Glacier (Fig. 1), shows evidence of subsurface undulations with an ablation area in the southeastern part of Schirmacher Glacier (Anschütz and others, 2007); these also contribute to

the reduction of velocity from north to south in the continental ice. Measured surface velocities for Schirmacher Glacier (with maximum velocity $\sim$11 m a^{-1}) are much lower than the velocities of Shirase Glacier (2700 m a^{-1}) which lies in a narrow trough less than 10 km wide (Pattyn and Derauw, 2002; Pattyn and Naruse, 2003). However, they are closer to those of Lambert Glacier (10–25 m a^{-1}) (Manson and others, 2000) and Potsdam Glacier (20–30 m a^{-1} at higher elevations and 70–80 m a^{-1} at lower elevations) (Dietrich and others, 1999; Anschütz and others, 2007) which also flow into ice shelves and which have similar surface trends.

As seen in Figure 5, the compressional strain rate in triangles A and C indicates blockage of the flow by the Schirmacher Oasis and presence of a nunatak near sites 05 and 06. The highest compression, in triangle M, is due to the resistance of Pevikhornet nunatak (near site 21). The north–south-trending compressional strain axes clearly indicate the role of the Schirmacher Oasis and nunataks in defining the compressive regime in Schirmacher Glacier. The highest extensional strain rates occur in triangle regions H, J, K, Q and R, which show the occurrence and contribution of steep and shallow criss-cross fracture zones and crevasses in the high-velocity region. The east–west to north-northeast trend of the extensional strain rates also follows the divergence of Schirmacher Glacier towards Nivlisen.

CONCLUSIONS

The velocity and strain distribution of Schirmacher Glacier have been investigated during two GPS campaigns during January to March, 2003 and 2004. The glacier velocity

Table 2. Principal strain rates with 1σ uncertainties and azimuth angles computed in the triangular regions shown in Figure 5; ε_{ext} and ε_{com} are extension and contraction strain rates, respectively, and ϕ is the azimuth of ε_{com}

Sub-network triangles	Barycentre		$\varepsilon_{ext} \pm 1\sigma$	$\varepsilon_{com} \pm 1\sigma$	$\phi \pm 1\sigma$
	Longitude	Latitude			
	°	°	$10^{-3}\,a^{-1}$	$10^{-3}\,a^{-1}$	°
A	11.57	−70.78	0.11 ± 0.01	0.84 ± 0.23	002.1 ± 0.9
B	11.48	−70.80	0.36 ± 0.21	0.31 ± 0.12	010.5 ± 1.0
C	11.53	−70.81	0.46 ± 0.25	0.72 ± 0.43	034.5 ± 8.6
D	11.48	−70.84	0.17 ± 0.04	0.15 ± 0.03	008.5 ± 4.8
E	11.57	−70.84	0.25 ± 0.15	0.26 ± 0.02	131.4 ± 1.3
F	11.61	−70.81	0.02 ± 0.01	0.05 ± 0.02	018.9 ± 3.8
G	11.64	−70.81	0.47 ± 0.07	0.04 ± 0.02	008.7 ± 4.1
H	11.67	−70.84	1.35 ± 0.62	0.42 ± 0.22	006.6 ± 1.0
I	11.71	−70.83	0.45 ± 0.04	0.34 ± 0.16	006.7 ± 1.7
J	11.73	−70.85	1.48 ± 0.85	0.55 ± 0.05	-49.9 ± 1.3
K	11.77	−70.83	1.34 ± 0.12	0.38 ± 0.08	015.2 ± 2.3
L	11.78	−70.88	0.43 ± 0.11	0.60 ± 0.06	100.1 ± 1.7
M	11.82	−70.92	0.57 ± 0.16	0.96 ± 0.16	-80.5 ± 1.2
N	11.53	−70.88	0.42 ± 0.10	0.27 ± 0.02	127.3 ± 9.0
O	11.47	−70.88	0.51 ± 0.39	0.05 ± 0.01	038.5 ± 2.9
P	11.63	−70.88	0.70 ± 0.18	0.34 ± 0.03	003.2 ± 1.0
Q	11.70	−70.91	1.28 ± 0.16	0.09 ± 0.01	117.6 ± 4.5
R	11.75	−70.90	1.01 ± 0.58	0.42 ± 0.08	037.2 ± 1.9

results show that the magnitude of the horizontal velocity is in the range 1.89–$10.88\,m\,a^{-1}$ with an average of $6.21\,m\,a^{-1}$, in the north-northeast direction. The distribution of velocity can be spatially correlated with topography, subsurface undulations, fractures/crevasses (coinciding with high velocities) and the influence of the blockage of Schirmacher Oasis. The surface strain analysis indicates that the region of extensional strain coincides with the surface gradient and crevasses, while the region of compressional strain is due to the blockage of Schirmacher Oasis and nunataks. The general trend to low (compared to other glaciers) velocities ($\sim11\,m\,a^{-1}$) is primarily attributed to the fact that Schirmacher Glacier is located in a region of exposed nunataks which extend along the ice-shelf grounding line.

GPR measurements can facilitate the detection of changes in the flow field, subglacial topography and internal structure of the glacier. To model glacier dynamics and estimate mass-balance change, a comprehensive knowledge of glacier geometry, boundary conditions, ice deformation and basal components of the glacier velocity is required. For studying the seasonal changes in velocity pattern, we propose to install continuous-recording GPS (with meteorological package) at selected sites on Schirmacher Glacier.

REFERENCES

Altamimi, Z., P. Sillard and C. Boucher. 2002. ITRF2000: a new release of the International Terrestrial Reference Frame for earth science applications. *J. Geophys. Res.,* **107**(B10), 2214. (10.1029/2001JB000561.)

Anschütz, H., H. Oerter, D. Steinhage and M. Scheinert. 2007. Investigating small-scale variations of the recent accumulation rate in Coastal Dronning Maud Land, East Antarctica. *Ann. Glaciol.,* **46**, 14–21.

Bassis, J.N., R. Coleman, H.A. Fricker and J.B. Minster. 2005. Episodic propagation of a rift on the Amery Ice Shelf, East Antarctica. *Geophys. Res. Lett.,* **32**(6), L06502. (10.1029/2004GLO22048.)

Bormann, P. and D. Fritzsche, eds. 1995. The Schirmacher Oasis, Queen Maud Land, East Antarctica, and its surroundings. *Petermanns Geogr. Mitt.* 289.

Damm, V. and D. Eisenburger. 2005. Ice thickness and subice morphology in central Queen Maud Land deduced by radio echo soundings (RES). *Geol. Jahrb.* **B97**, 109–127.

Davies, K. and G.K. Hartmann. 1997. Studying the ionosphere with the Global Positioning System. *Radio Sci.,* **32**(4), 1695–1704.

Dietrich, R., R. Metzig, W. Korth and J. Perlt. 1999. Combined use of field observations and SAR interferometry to study ice dynamics and mass balance in Dronning Maud Land, Antarctica. *Polar Res.,* **18**(2), 291–298.

Dong, D., T.A. Herring and R.W. King. 1998. Estimating regional deformation from a combination of space and terrestrial geodetic data. *J. Geod.,* **72**(4), 200–214.

Feigl, K.L., R.W. King and T.H. Jordan. 1990. Geodetic measurement of tectonic deformation in the Santa Maria fold and thrust belt, California. *J. Geophys. Res.,* **95**(B3), 2679–2699.

Feigl, K.L. *and 14 others.* 1993. Space geodetic measurement of crustal deformation in central and southern California, 1984–1992. *J. Geophys. Res.,* **98**(B12), 21,677–21,712.

Fricker, H.A., N.W. Young, R. Coleman, J.N. Bassis and J.B. Minster. 2005. Multi-year monitoring of rift propagation on the Amery Ice Shelf, East Antarctica. *Geophys. Res. Lett.,* **32**(2), L02502 (10.1029/2004GLO21036.)

Gloersen, P. and W.J. Campbell. 1988. Variations in Arctic, Antarctic, and global sea ice covers during 1978–1987 as observed with the Nimbus 7 scanning multichannel microwave radiometer. *J. Geophys. Res.,* **93**(C9), 10,666–10,674.

Goldstein, R.M., H. Engelhardt, B. Kamb and R.M. Frolich. 1993. Satellite radar interferometry for monitoring ice sheet motion: application to an Antarctic ice stream. *Science,* **262**(5139), 1525–1530.

Hermichen, W.D. 1995. The continental ice cover in the surroundings of the Schirmacher Oasis. *In* Bormann, P. and D. Fritzsche, *eds.* The Schirmacher Oasis, Queen Maud Land, East Antarctica, and its surroundings. (*Petermanns Geogr. Mitt.* 289, 221–242.

Herring, T.A. 2002. *GLOBK global Kalman filter VLBI and GPS analysis program, version 10.0.* Cambridge, MA, Massachusetts Institute of Technology.

Herring, T.A. and R.W. King. 1990. Geodesy by radio interferometry: the application of Kalman filtering to the analysis of very long baseline interferometry data. *J. Geophys. Res.,* **95**(B8), 12,561–12,581.

Horwath, M. *and 7 others.* 2006. Nivlisen, an Antarctic ice shelf in Dronning Maud Land: geodetic–glaciological results from a combined analysis of ice thickness, ice surface height and ice-flow observations. *J. Glaciol.,* **52**(176), 17–30.

Joughin, I., E. Rignot, C.E. Rosanova, B.K. Lucchitta and J. Bohlander. 2003. Timing of recent accelerations of Pine Island Glacier, Antarctica. *Geophys. Res. Lett.,* **30**(13), 1706. (10.1029/2003GL017609.)

King, M. 2001. The dynamics of the Amery Ice Shelf from a combination of terrestrial and space geodetic data. (PhD thesis, University of Tasmania.)

King, M. 2004. Rigorous GPS data processing strategies for glaciological applications. *J. Glaciol.,* **50**(171), 601–607.

King, R.W. and Y. Bock. 2002. *Documentation for the GAMIT GPS analysis software, release 10.0.* Cambridge, MA, Massachusetts Institute of Technology.

King, M., R. Coleman and L.N. Nguyen. 2003. Spurious periodic horizontal signals in sub-daily GPS position estimates. *J. Geod.,* **77**(1–2), 15–21.

Korth, W. and R. Dietrich. 1996. Ergebnisse geodätischer Arbeiten Gebiet der Schirmacher oase/Antarktika 1988–1993. Bayer. Akad. Wiss., Deut. Geod. Komm. B301.

Lawver, L.A., L.M. Cahagan and M.F. Coffin. 1992. The development of paleoseaways around Antarctica. *In* Kennett, J.P. and D.A. Warnke, *eds. The Antarctic paleoenvironment: a perspective on global change, Part 1.* Washington, DC, American Geophysical Union. (Antarctic Research Series 56.)

Leibert, J. and G. Leonhardt. 1973. Astronomic observations for determining ice movements in the Vostok Station area. *Sov. Antarct. Exped. Inf. Bull.,* **88**, 68–70.

Leick, A. 1995. *GPS satellite surveying. Second edition.* New York, etc., John Wiley and Sons Inc.

Manson, R., R. Coleman, P. Morgan and M. King. 2000. Ice velocities of the Lambert Glacier from static GPS observations. *Earth, Planets Space,* **52**(11), 1031–1036.

Meir, M.F. 1993. Ice, climate and sea level: do we know what is happening? *In* Peltier, W.R., *ed. Ice in the climate system.* Berlin, etc., Springer-Verlag, 141–160. (NATO ASI Series I: Global Environmental Change 12.)

Metzig, R., R. Dietrich, W. Korth, J. Perlt, R. Hartmann and W. Winzer. 2000. Horizontal ice velocity estimation and grounding zone detection in the surroundings of Schirmacheroase, Antarctica, using SAR interferometry. *Polarforschung,* **67**(1–2), 7–14.

Meyer, U., D. Steinhage, U. Nixdorf and H. Miller. 2005. Airborne radio echo sounding survey in Central Dronning Maud Land, East Antarctica. *Geol. Jahrb.,* **B97**, 129–140.

Pattyn, F. and D. Derauw. 2002. Ice-dynamic conditions of Shirase Glacier, Antarctica, inferred from ERS-SAR interferometry. *J. Glaciol.,* **48**(163), 559–565.

Pattyn, F. and R. Naruse. 2003. The nature of complex ice flow in Shirase Glacier catchment, East Antarctica. *J. Glaciol.,* **49**(166), 429–436.

Ravindra, R., A. Chadurvedi and M.J. Beg. 2002. Melt water lakes of Schirmacher Oasis – their genetic aspects and classification. *In* Sahoo, D. and P.C. Pandey, *eds. Advances in marine and Antarctic science.* New Delhi, APH Publishing Corporation.

Rignot, E., G. Casassa, P. Gogineni, W. Krabill, A. Rivera and R. Thomas. 2004. Accelerated ice discharge from the Antarctic Peninsula following the collapse of Larsen B ice shelf. *Geophys. Res. Lett.,* **31**(18), L18401. (10.1029/2004GL020697.)

Sengupta, S. 1986. Geology of Schirmacher Range (Dakshin Gangotri), East Antarctica. *Third Indian Expedition to Antarctica, Scientific Report. New Dehli, Department of Ocean Development,* 187–217. (Tech. Publ. No. 3.)

Serpelloni, E., M. Anzidei, P. Baldi, G. Casula and A. Galvani. 2005. Crustal velocity and strain-rate fields in Italy and surrounding regions: new results from the analysis of permanent and non-permanent GPS networks. *Geophys. J. Int.,* **161**(3), 861–880.

Testut, L., R. Hurd, R. Coleman, F. Rémy and B. Legrésy. 2003. Comparison between computed balance velocities and GPS measurements in the Lambert Glacier basin, East Antarctica. *Ann. Glaciol.,* **37**, 337–343.

Vey, S. *and 10 others.* 2002. GPS measurements of ocean loading and its impact on zenith tropospheric delay estimates: a case study in Brittany, France. *J. Geod.,* **76**(8), 419–427.

Wingham, D.J., A.L. Ridout, R. Scharroo, R.J. Arthern and C.K. Shum. 1998. Antarctic elevation change from 1992 to 1996. *Science,* **282**(5388), 456–458.

Zwally, H.J. *and 15 others.* 2002. ICESat's laser measurements of polar ice, atmosphere, ocean and land. *J. Geodyn.,* **34**(3–4), 405–445.